

# How does downsampling affect needle electromyography signals? A generalisable workflow for understanding downsampling effects on high-frequency time series

Mathieu J.L. Cherpitel<sup>1</sup>, Janne A.M. Luijten<sup>2,3</sup>, Thomas H.W. Bäck<sup>1</sup>, Camiel Verhamme<sup>3</sup>, Martijn R. Tannemaat<sup>2</sup>, and Anna V. Kononova<sup>1</sup>

<sup>1</sup>*Leiden Institute of Advanced Computer Science, Leiden, The Netherlands*

<sup>2</sup>*Leiden University Medical Centre, Department of Neurology, Leiden, The Netherlands*

<sup>3</sup>*Amsterdam University Medical Centre, Department of Neurology, Amsterdam, The Netherlands*

## Abstract

Automated analysis of needle electromyography (nEMG) signals is emerging as a tool to support the detection of neuromuscular diseases (NMDs), yet the signals' high and heterogeneous sampling rates pose substantial computational challenges for feature-based machine-learning models, particularly for near real-time analysis. Down-sampling offers a potential solution, but its impact on diagnostic signal content and classification performance remains insufficiently understood. This study presents a workflow for systematically evaluating information loss caused by downsampling in high-frequency time series. The workflow combines shape-based distortion metrics with classification outcomes from available feature-based machine learning models and feature space analysis to quantify how different downsampling algorithms and factors affect both waveform integrity and predictive performance. We use a three-class NMD classification task to experimentally evaluate the workflow. We demonstrate how the workflow identifies downsampling configurations that preserve diagnostic information while substantially reducing computational load. Analysis of shape-based distortion metrics showed that shape-aware downsampling algorithms outperform standard decimation, as they better preserve peak structure and overall signal morphology. The results provide practical guidance for selecting downsampling configurations that enable near real-time nEMG analysis and highlight a generalisable workflow that can be used to balance data reduction with model performance in other high-frequency time-series applications as well.

## 1 Introduction

Needle electromyography (nEMG) is a diagnostic technique for neuromuscular disorders (NMDs). NMDs are diseases affecting muscles, nerves or motor neurons that cause weakness or sensory deficits [1]. Timely and accurate diagnosis of NMDs is becoming more important as more treatments for various NMDs are rapidly emerging [2–4]. During nEMG examination, a needle electrode is inserted into the muscle to evaluate its electrical activity at rest and during voluntary contraction. Interpretation of the nEMG is performed in real-time by a clinical neurophysiologist through audio-visual assessment of the signal [5]. Even with adequate training and expertise, the interpretation of nEMG signals remains inherently subjective, varies across medical centres and can potentially result in limited agreement among different clinicians [6].

To address these limitations, several studies have developed machine learning (ML) approaches to support or automate nEMG interpretation [7]. Feature-based ML approaches, in particular, offer superior explainability compared to deep learning approaches and have shown

promising results in neurophysiological applications [7–9]. The drawback of these feature-based ML approaches, however, is the need for extensive feature extraction before classification. Together with the high temporal resolution of nEMG signals, this poses a computational challenge and hinders (near) real-time analysis and, thus, clinical implementation.

A possible strategy to mitigate this issue is to reduce the temporal resolution of the signal by using downsampling before applying feature extraction methods. However, downsampling introduces another trade-off: reducing the temporal resolution is only appropriate when the essential (diagnostic) information embedded in the signal is preserved.

Previous studies within the biomedical field have explored downsampling in electroencephalography (EEG) [10], the electrocardiogram (ECG) [11, 12], and surface EMG [13, 14]. Collectively, these studies show that the impact of downsampling varies widely: it can reduce classification accuracy [10], while it may also preserve [11] or even enhance [12, 13] classification performance while reducing computational load. Using

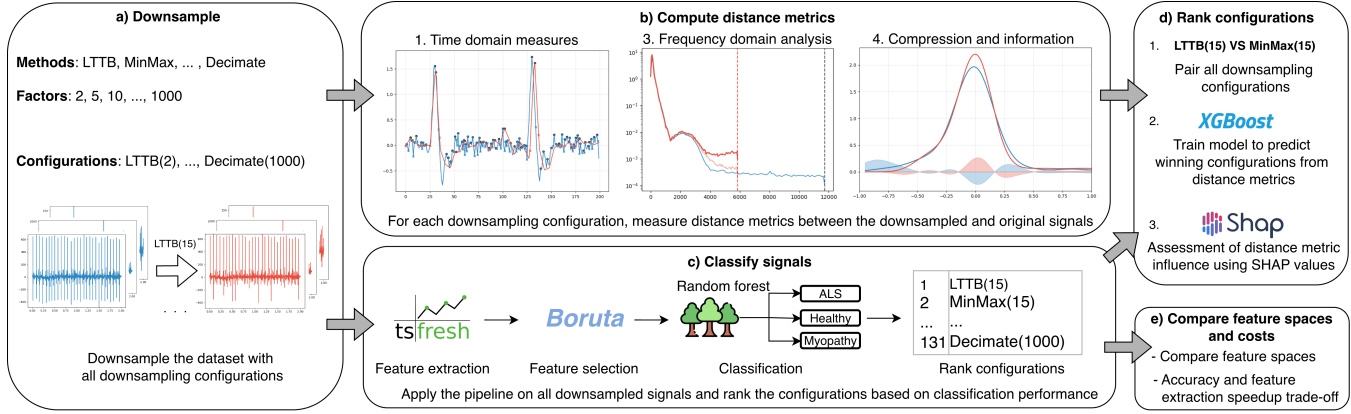


Figure 1: Five steps of the proposed workflow to investigate the effects of downsampling on time series.

seven datasets from within and beyond the biomedical field, Moltó-Gallego et al. similarly reported that downsampling impact varies across extracted features, downsampling method, and analysed dataset [15]. Additionally, they further demonstrated that downsampling can, in specific scenarios, simultaneously improve classification performance and reduce computational load.

While downsampling is a widely recognised strategy to reduce computational load, its application across studies is non-standardised, and a systematic evaluation method to determine acceptable levels of information loss is lacking. This paper addresses this gap. It is organised as follows: Section 2 presents a workflow that combines shape-based distortion metrics, classification performance, and feature space analysis to assess how downsampling affects high-resolution time series. In Section 3, we apply this workflow to a three-class nEMG problem and present the specific results of that evaluation, including the effects on computational load. Section 4 discusses our results and reflects on the general applicability of the proposed workflow. Section 5 concludes the paper and outlines the implications of our results for clinical implementation of nEMG analysis pipelines.

## 2 Methods

The proposed workflow to investigate the effects of downsampling on time series consists of five main steps, summarised in Figure 1 and elaborated in this section.

- We first define several downsampling configurations, each combining an algorithm and a downsampling factor. Each configuration is then applied to all signals in the dataset, resulting in one downsampled dataset per considered configuration.
- We then compute a selection of distance metrics between each downsampled signal and its corresponding original signal for each configuration.

- In parallel, we train an automated time series classification pipeline on each dataset. This pipeline was originally designed to process vehicle crash data [16, 17] and proved to offer good performance on a variety of clinically meaningful time series data, including EEG [18] and nEMG [19]. Once the pipeline is trained on each dataset separately, we evaluate the classification performances and rank the configurations according to the achieved accuracies.
- Using the distance metrics and the classification performance based ranks, we train a ranking model to predict the best downsampling configurations from distance metrics alone. From this model, we extract SHAP values to interpret the contributions of individual distance metrics to identify key signal characteristics that the classifier relies on.
- Finally, we compare the feature spaces obtained from each dataset to analyse how they get altered across downsampling configurations. We report the reduction in feature extraction time and its trade-off with classification accuracy.

### 2.1 Downsample

Downsampling reduces the temporal resolution of a time series through the selection of a subset of points. Given a time series  $X = [x_1, x_2, \dots, x_N]$ , the downsampled version is defined as:

$$X' = d(X, k)$$

where  $d$  denotes the downsampling algorithm and  $k$  the downsampling factor. The resulting signal  $X'$  has a length  $|X'| \approx \lfloor N/k \rfloor$ , with both dimensionality and sampling frequency reduced by approximately a factor  $k$ .

Although the most common approach to downsampling is a simple Decimate (retaining every  $k$ -th point), we also evaluate algorithms developed for data visualisation (MinMax, M4, LTTB and MinMaxLTTB). Since nEMG

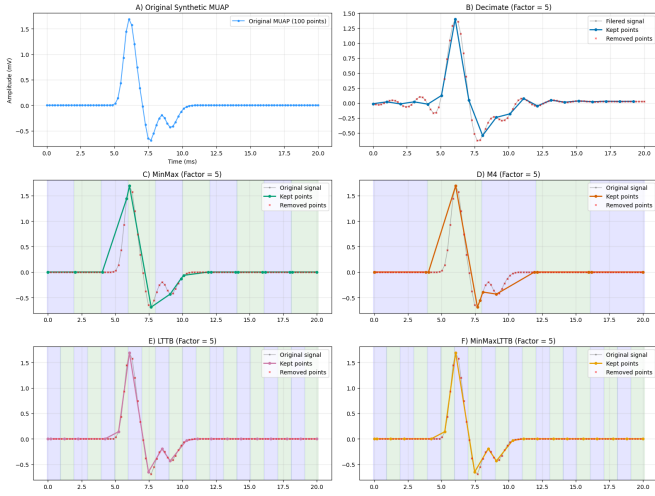


Figure 2: Effects of five downsampling methods on a synthetic MUAP-like waveform. Shaded regions indicate the value groups (when applicable) used by each algorithm. Typical effects are visible: **B**) Decimate preserves MUAP duration but loses peak amplitude and phase detail. **C**) MinMax preserves amplitude and duration but alters phase count. **D**) M4 maintains amplitude but distorts duration and phases. **E**) and **F**) LTTB and MinMaxLTTB yield the most faithful approximations, preserving amplitude, duration, and phase structure.

signals are traditionally audio-visually assessed, attempting to maintain their visual shape could preserve information content. These algorithms use groups of values from which a set number of points are kept based on their rules. In this case, the downsampling factor determines the size of the groups of values.

To illustrate the behaviour of the investigated algorithms, we generate a synthetic waveform resembling a motor unit action potential (MUAP) and apply each algorithm, yielding their respective downsampled versions. Figure 2 shows the results for the five investigated algorithms:

- **Decimate:** Standard decimation by retaining every  $n$ th point after applying an anti-aliasing filter.
- **MinMax:** This method retains extreme values by returning the  $\min$  and  $\max$  point from each group, aiming to preserve the overall amplitudes of the signal.
- **M4:** Proposed by Jugel et al. [20], this algorithm aims to avoid pixel representation errors that can occur when using MinMax. By ignoring the transitions between groups, the line drawn between two extrema can include a pixel that was not used in the original representation of the data, resulting in a representation error. To overcome this problem, the algorithm selects both the boundaries (*first, last*) and the extreme values ( $\min, \max$ ) of each group to ensure an accurate connection between groups. This approach requires groups twice the size of those for

MinMax since the number of selected values increases from two to four. If the same point is selected multiple times (e.g., the last value is also the maximum), fewer than four points are kept.

- **LTTB:** The Largest Triangle Three Buckets method, proposed by Steinarsson [21], quantifies point influence by maximising the *effective area*, i.e. the area of the triangle formed by the evaluated point, the point selected in the previous group, and the median of the next group. This technique is widely adopted in data visualisation due to its accurate approximation of signal shape.
- **MinMaxLTTB:** Introduced by Van de Donckt et al. [22], this variant reduces the computational cost of LTTB by pre-selecting vertical extremes ( $\min, \max$ ) before applying LTTB. The ratio controlling the number of points retained before LTTB can be adjusted. Following the author’s suggestions, we use a pre-selection ratio of 4.

It is standard practice to apply an anti-aliasing filter before downsampling with the decimate algorithm to prevent high-frequency components from being misrepresented as lower-frequency components after downsampling. We used the `scipy.signal.decimate` function with a default FIR low-pass filter with zero phase. For the group methods, however, anti-aliasing filters remove signal features that these algorithms are designed to preserve: sharp peaks and vertical extrema. The filter will reduce the true maximum and increase the true minimum, yielding downsampled signals with underestimated peak-to-peak amplitudes. Since MinMax and M4 explicitly try to preserve these extremes ( $\min, \max$ ), the filter corrupts the data they are intended to select. LTTB and MinMaxLTTB select points that maximise the effective area, which translates to prioritising points that define the sharpest turns or extremes in the signal shape. As these group methods do not sample uniformly, they inherently distort the signal’s original frequency characteristics. Therefore, applying low-pass filtering before these algorithms provides no benefit and instead induces artificial smoothing.

Given a dataset  $\mathcal{X} = \{X_1, X_2, \dots, X_M\}$  of  $M$  time series, a set of downsampling methods  $\mathcal{D}$  and factors  $\mathcal{K}$ , each unique configuration  $(d, k)$  with  $d \in \mathcal{D}$  and  $k \in \mathcal{K}$ , is applied to all time series in the dataset. The complete collection of downsampled datasets is then:

$$\{\mathcal{X}_{(d,k)} \mid d \in \mathcal{D}, k \in \mathcal{K}\},$$

Which, in addition to the original dataset, serves as input for subsequent distance metric analysis and classification.

## 2.2 Compute Distance Metrics

To assess the impact of downsampling on the shape of our signals, we compute several distance metrics between each

original signal and its corresponding downsampled version for all configurations. We selected metrics from the time domain, frequency domain, and information theory that capture key signal characteristics potentially affected by downsampling. The objective is to identify computationally efficient measures of information loss and signal distortion without requiring the full classification pipeline to be run for all configurations. The selected metrics are described in Table 1. They will be used to identify signal characteristics that are important for the classification model and which downsampling methods best preserve them.

### 2.3 Classify signals

The third step of our workflow evaluates how well downsampled signals support an automated analysis task. This step can be adapted to various tasks (e.g., classification, regression, or anomaly detection), depending on the research objective. For this study, we focus on a supervised classification task supported by an automated time series classification pipeline [16], which consists of the following steps: 1) We extract features from each signal with *tsfresh* by Christ et al. [24]; 2) The extracted features are passed to the *Boruta* algorithm [25] for feature selection. To promote stable feature selection in the presence of class imbalance, *Boruta* is applied within a stratified k-fold cross-validation framework; 3) The selected features are used to train and validate a random forest classifier using the previously generated cross-validation folds, allowing us to assess feature importances using both Mean Decrease in Impurity (MDI) and a permutation-based method.

Classification performance was evaluated using accuracy, F1-score, precision, recall, and ROC AUC computed one-vs-rest (OvR). In addition to overall performance, we measured per-class sensitivity and specificity to assess the effects of downsampling on each class. The parameters used for cross-validation, *Boruta*, and the random forest classifier are detailed in the experimental evaluation section. After reporting the classification performance of each dataset on the validation splits, configurations were ranked based on their achieved accuracy scores.

### 2.4 Rank configurations

To further understand the effects of downsampling, we train a ranking model using *XGBoost* [26] to correlate distance metrics with classification performance. The objective is to identify which metrics best capture signal characteristics most relevant to the classifier, indicated by deterioration in classification accuracy.

Since training the complete pipeline to obtain the classification accuracy of each configuration is computationally expensive, we cannot generate enough samples to properly train a regression model directly predicting classification accuracy from the distance metrics. Instead, we adopt a pairwise ranking approach, which allows the

model to learn relative performance between configurations from a limited number of evaluated samples. In this approach, all possible non-repetitive configuration pairs are generated. Each comparison is then used as a sample, consisting of the difference between the distance metrics of the two configurations and a binary label: 1 if the first configuration achieves a higher classification accuracy than the second (configuration 1 wins), and 0 otherwise (configuration 1 loses). In pairwise ranking, the achieved rank of a configuration is determined by the number of victories it obtains. Since each configuration is compared to all others, this ensures an accurate overall ranking. Once the *XGBoost* model is trained, we extract SHAP values to evaluate the contributions of each distance metric.

#### 2.4.1 Evaluation of pairwise comparisons and consequent ranking

The pairwise ranking approach consists of creating non-repetitive pairs, predicting the winner of each pair, and ranking the configurations based on the number of victories. To evaluate the performance of a model trained for this purpose, two approaches can be used: (1) how often the model correctly identifies the winner (i.e., the configuration with the higher classification accuracy), and (2) how accurate the final ranking is. For the latter, a correlation measure called *Kendall's  $\tau$*  assesses ordinal association between two quantities, capturing the similarity of their ordering. When evaluating how well the model predicts the correct winner, it is important to note that not all pairwise comparisons are equally difficult or relevant. To obtain an accurate ranking, all possible pairs must be considered. Consequently, some pairs involve configurations with very different downsampling factors, resulting in large differences in distance metrics and making correct classification trivial. To avoid overestimating the performance of the *XGBoost* model due to these easy comparisons, we calculate the weighted *XGBoost* accuracy based on an exponential decay of the difference in random forest classification accuracy. Pairs with smaller differences in random forest classification accuracy receive higher weights, increasing their impact on the weighted XGBoost accuracy.

For each pair  $(i, j)$ , let the difference in performance be:

$$\Delta_k = |\text{acc}_i - \text{acc}_j|$$

A weight is assigned to each pair, using a decaying exponential function:

$$w_k = e^{-\lambda \Delta_k}$$

and the weighted accuracy of *XGBoost* is measured as:

$$\text{Weighted accuracy} = \frac{\sum_k w_k C_k}{\sum_k w_k}$$

Where  $C_k$ , the correctness, is equal to 1 if the model predicted correctly and 0 otherwise, and  $\lambda$  is the decay rate of the weights.

Table 1: Overview of the distance metrics used to compare original and downsampled signals.

Distance metric	Type	Formula
Root Mean Squared Error (RMSE)	Time domain	$RMSE(X, Y) = \sqrt{\frac{1}{N} \sum_{i=1}^N (x_i - y_i)^2} \quad (1)$
Normalised Mean Squared Error (NMSE)	Time domain	$NMSE(X, Y) = \frac{\sum_{i=1}^N (x_i - y_i)^2}{\sum_{i=1}^N (x_i - \bar{x})^2} \quad (2)$
Pearson Correlation Coefficient (PCC)*	Time domain	$PCC(X, Y) = \frac{\sum_{i=1}^n (x_i - \bar{x})(y_i - \bar{y})}{\sqrt{\sum_{i=1}^n (x_i - \bar{x})^2} \sqrt{\sum_{i=1}^n (y_i - \bar{y})^2}} \quad (3)$
Spearman Correlation Coefficient (SCC)*	Time domain	$SCC(X, Y) = PCC(R(X), R(Y)) \quad (4)$
Pearson Envelope Correlation*	Time domain	$PCC(\mathcal{H}(X), \mathcal{H}(Y)) \text{ and } SCC(\mathcal{H}(X), \mathcal{H}(Y)) \quad (5)$
Zero Crossing Rate (ZCR)**	Time domain	$ZCR(X) = \frac{1}{ X  - 1} \sum_{t=1}^{ X -1}  s[x(t)] - s[x(t-1)]  \quad (6)$
Peaks count**	Time domain	$\#peaks(X) \text{ (scipy find_peaks, default params)} \quad (7)$
Skewness**	Time domain	$Skew(X) = \frac{\frac{1}{N} \sum_{i=1}^N (x_i - \bar{x})^3}{(std(X))^3} \quad (8)$
Kurtosis**	Time domain	$Kurt(X) = \frac{\frac{1}{N} \sum_{i=1}^N (x_i - \bar{x})^4}{(std(X))^4} \quad (9)$
Euclidean distance of PSDs	Frequency domain	$PSD_{eucl}(X, Y) = \sqrt{\sum_{i=1}^{N_f} (P_X(f_i) - P_Y(f_i))^2} \quad (10)$
Normalised Compression Distance (NCD)	Info theory	$NCD(X, Y) = \frac{Z(XY) - \min(Z(X), Z(Y))}{\max(Z(X), Z(Y))} \quad (11)$
Jensen-Shannon Divergence (JSD)	Info theory	$JSD(P  Q) = \frac{1}{2}D_{KL}(P  M) + \frac{1}{2}D_{KL}(Q  M) \quad (12)$

\*For consistency, correlation measures were inverted, so that lower values always indicate greater similarity, aligning them with the other distance-based metrics.

\*\*Distance computed as absolute difference:  $d(X, Y) = |f(X) - f(Y)|$  where  $f$  is the respective metric.

(4):  $R(X)$  denotes the ranks of elements in  $X$  sorted in ascending order.

(5):  $\mathcal{H}$  denotes the Hilbert transform for envelope extraction before measuring the Pearson correlation.

(6):  $s(x) = 1$  if  $x \geq 0$  else 0.

(7): With scipy v 1.14.1.

(10): Where  $P_X(f_i)$  and  $P_Y(f_i)$  are the values of the normalised Power Spectral Densities (PSDs) of signal  $X$  and  $Y$  at frequency bin  $f_i$  estimated with the Welch method.  $N_f$  is the total number of bins.

(11):  $Z$  approximates Kolmogorov complexity via gzip compression [23].

(12):  $D_{KL} =$  Kullback-Leibler divergence,  $M = \frac{1}{2}(P + Q)$ . PDFs estimated via histogram discretisation.

## 2.5 Compare feature spaces and costs

Since we use a feature-based classifier, this final step analyses how downsampling affects the high-dimensional feature spaces and computational cost associated with feature extraction. We use four techniques:

- **Feature Importance Shifts:** Following classification, we obtain a vector for each feature, representing its importances across folds. To compare how feature importances change across downsampling configurations, the fold-averaged importances of the features are clustered using  $k$ -means clustering. The resulting clusters exhibit the global behaviour of feature groups and allow for interpreting shifts in feature relevance.
- **Feature Selection Stability:** Feature selection is performed over multiple folds of cross-validation. To assess the stability of the selected feature set, we measure the selection frequency of features across folds. The *Jaccard index*, a quantitative stability measure, is computed to assess the stability across folds.
- **Feature Importance Trajectories:** To visualise how feature importance evolves as the downsampling factor increases, the importance vectors for all configurations are projected to a lower-dimensional embedded space using dimensionality reduction techniques (e.g., MDS, t-SNE). This projection enables visualising trajectories for each downsampling algorithm, revealing how the feature relevance structure shifts as the downsampling factor increases.
- **Feature Extraction Speedup:** The primary benefit of downsampling is the reduction in feature extraction time. We measure feature extraction time  $t_{ds}$  for each downsampling configuration. The speedup  $S$  achieved is quantified by the ratio of the feature extraction time of the original signal ( $t_{orig}$ ) to the downsampled signal:  $S = t_{orig}/t_{ds}$ . This provides a representative measure of the computational gain, enabling assessment of the trade-off with classification performance.

This analysis focuses on feature importances because the large variability of feature values between samples complicates direct interpretation.

## 3 Experimental Evaluation

To illustrate and evaluate the workflow proposed in Section 2, we apply it to the EMGLAB dataset. The following subsections describe the dataset used, the experimental setup, and the obtained results.

Table 2: Distribution of labels in the EMGLAB dataset.

Label	Control	Myopathic	ALS
Number of patients	9	6	7
Number of recordings	270	107	98

### 3.1 Data

To assess the impact of downsampling on nEMG, we use the EMGLAB dataset, as it provides high-quality, annotated contraction segments that facilitate the analysis of motor unit activity. The data was collected from the Department of Clinical Neurophysiology of Rigshospitalet, Copenhagen, for a study on signal decomposition and firing patterns analysis [27]. It has been shared publicly and is commonly used in a wide variety of studies due to its ease of use and the difficulty in obtaining other labelled nEMG signals. A scoping review by De Jonge et al. [7] identified a total of 31 out of 51 papers that used EMGLAB as their primary dataset to develop artificial intelligence applications. Signals were recorded using a concentric needle inserted into the biceps brachii of 22 patients at a low voluntary level of contraction. All signals consist of 262124 measurements sampled at 23437.5 Hz (approximately 11 seconds). High- and low-pass filter boundaries were set to 2 Hz and 10 kHz, respectively. The distribution of labels across patients is relatively balanced with 9 control, 6 myopathic and 7 amyotrophic lateral sclerosis (ALS) patients. However, the number of recordings per patient differs largely between the labels: each control subject has 30 recordings, whereas the number of recordings for myopathic and ALS patients varies between 2 and 25 per patient. As a result, the dataset has an imbalance factor of 2.76 for the control label (see Table 2). The diagnostic labels were confirmed using both clinical and electrophysiological signs.

### 3.2 Experimental setup

The five investigated downsampling algorithms ( $\mathcal{D}$ ) introduced in Section 2.1 have been implemented in a Python library by Van de Donckt et al [28], called *tsdownsample*. These algorithms were selected as they each have unique characteristics that will result in diverse signal representations. To explore a wide range of possibilities while maintaining computational feasibility, we selected 26 downsampling factors ( $\mathcal{K}$ ). The selected factors provide dense coverage of potentially optimal downsampling factors at the lower end of the spectrum (2–100), while also including higher values (200–1000) to evaluate the effects of extreme downsampling:

$$\mathcal{D} = \{\text{Decimate, M4, MinMax, LTTB, MinMaxLTTB}\}$$

$$\mathcal{K} = \{2, 5, 10, 15, \dots, 95, 100, 200, 300, 400, 500, 1000\}$$

We report a summary of the hyperparameters used in the classification pipeline for our experiment in Table 3.

Table 3: Summary of hyperparameters used in the classification pipeline.

Parameter Group	Value
<b>Cross-validation settings</b>	
Number of folds	10
Split type	Stratified $k$ -fold
<b>Boruta settings</b>	
Number of iterations	100
<b>Random Forest settings</b>	
Number of estimators	200
Maximum depth	None
Minimum samples per split	2
Minimum samples per leaf	1

For this experiment, we use the *EfficientFC* features set from *tsfresh* since it includes a large quantity of features (777) while excluding the ones flagged with a high computational cost.

### 3.3 Classification performance across configurations

As done in the previous use of the classification pipeline [19], we splitted the EMGLAB recordings into two-second segments. We then downsampled them, extracted *tsfresh* features, reduced the set using *Boruta*, and trained the random forest classifier. Performance was evaluated for each configuration using 10-fold cross-validation. To assess the classifier’s robustness to signal downsampling, we conducted a Friedman test with Nemenyi post-hoc analysis. We defined the critical downsampling factor for each algorithm as the first point at which the algorithm’s accuracy was statistically different ( $p < 0.05$ ) from that obtained on the original, non-downsampled data (Figure 3).

Results show that M4 and Decimate maintained original performance below a downsampling factor of 10, while MinMax preserved accuracy below a factor of 25. LTTB and MinMaxLTB maintained a classification accuracy similar to original below factor 35. Although the performance curves of Decimate and MinMax appear similar in Figure 3, the difference in critical factors arises from the statistical test’s sensitivity to variance: Decimate’s consistent lower ranking at factor 10 reached statistical significance, while MinMax’s higher ranking in some folds delayed the critical difference until factor 25.

To further investigate the change in classification performance, we measure per-class sensitivity and specificity (Figure 4). LTTB and MinMaxLTB consistently achieved superior scores across all classes. However, all algorithms exhibited a critical, systematic reduction in control class specificity as the downsampling factor increased. This decline corresponds to a rise in false positives for the Control class, indicating a bias towards the

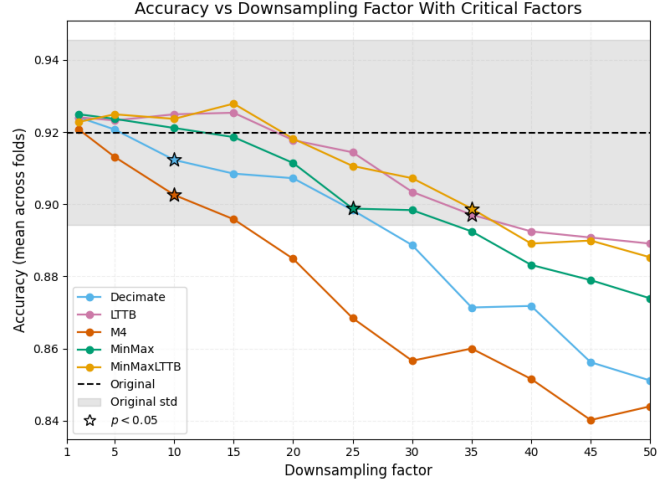


Figure 3: Accuracy per downsampling factor on the EMGLAB dataset after downsampling. Each line represents a downsampling algorithm, and the highlighted stars indicate the critical factor ( $p < 0.05$ ) for each algorithm. The horizontal dashed line corresponds to the ROC AUC achieved on the original (non-downsampled) data, and the grey area represents its standard deviation across the 10 folds of cross-validation. Stars represent for each algorithm the first factor with a critical difference in classification accuracy.

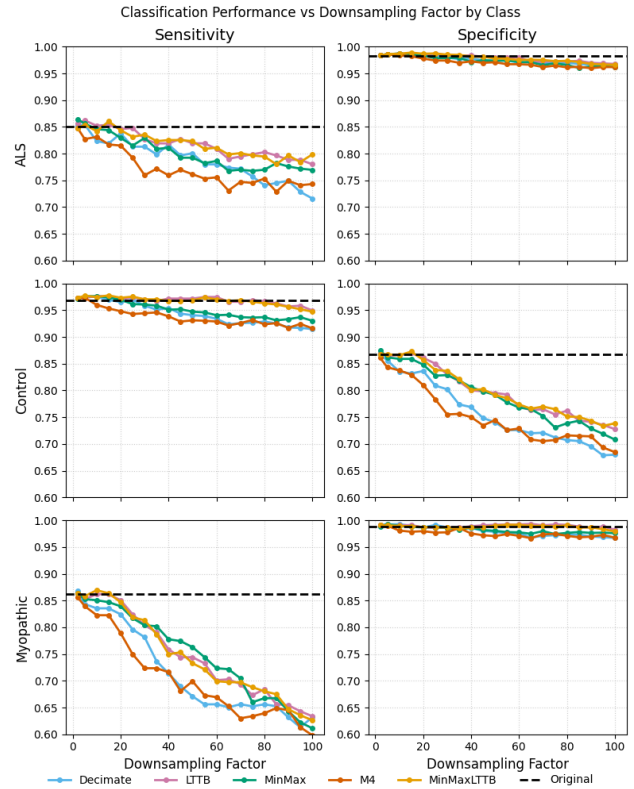


Figure 4: Measured per-class performance for each downsampling configuration. MinMaxLTB and LTTB achieved higher sensitivity and specificity over all classes. All algorithms greatly reduced the specificity towards the Control class, indicating that the model defaults to predicting Control when the signal information content is damaged.

over-represented Control label when features are compromised. Consequently, the high overall accuracy achieved at extreme downsampling factors is misleading, as it hides a critical failure to correctly identify the minority classes (ALS and Myopathic), which are crucial for this task. Therefore, in addition to classification accuracy, per-class metrics should be investigated to assess the impact of downsampling.

### 3.4 Ranking model results

The ranking model achieved a high *Kendall's  $\tau$*  of 0.953, demonstrating that distance metrics alone enable reliable ranking of downsampling configurations and distinguish beneficial signal approximations from harmful distortions. This was further supported by high weighted accuracies (0.969, 0.965, and 0.956 for decay rate of the weights:  $\lambda = 5, 10, 20$ ), demonstrating robustness even in challenging comparisons with small classification accuracy differences. Since the model's predictions rely on distance metrics, the SHAP analysis (Figure 5) reveals which measures of shape distortion are most informative for favourable downsampling. The most predictive metric is the Pearson envelope correlation using the Hilbert transform. Its high importance indicates the random forest's sensitivity to changes in overall signal amplitude. In contrast, a "good" (in this case, low) Euclidean Power Spectral Density (PSD) distance is associated with poor performance, suggesting that modifications in the frequency domain do not negatively impact the random forest's accuracy. Both Kurtosis and Skewness were positive indicators of downsampling quality, meaning that preservation of the signal's amplitude distribution is a desirable property for a downsampling algorithm. Conversely, the Zero Crossing Rate can be considered unreliable as an indicator of downsampling quality, indicating that the model does not rely on changes near zero to classify signals. Figure 6 shows how downsampling affects both high-frequency components and signal morphology.

### 3.5 Effects of downsampling on the feature space

As per the methodology detailed in Section 2.5, we analysed how downsampling affects the high-dimensional feature spaces and computational cost associated with feature extraction.

#### 3.5.1 Feature importance shifts

To analyse how the importance of different features evolved across downsampling configurations, we clustered the fold-averaged feature importance vectors using  $k$ -means clustering. Silhouette analysis revealed that five clusters best represent the evolution of feature importance for increasing downsampling factors; their trajectories are presented in Figure 7.

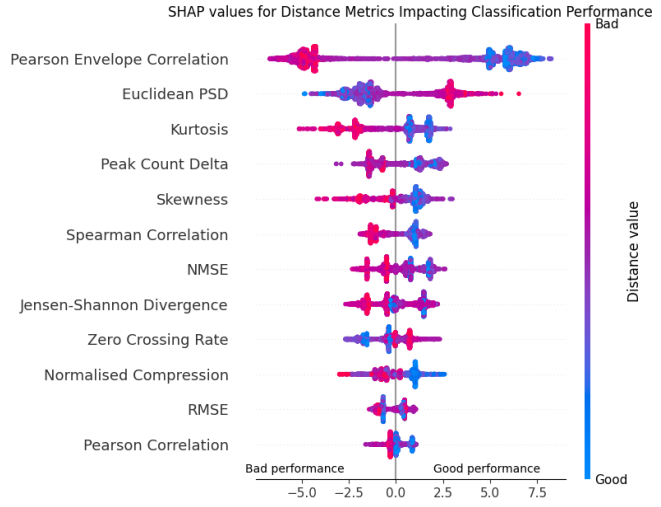


Figure 5: Reported SHAP values for the distance metrics used to predict winning downsampling configuration. For interpretability, the colour scale corresponds to the degree of similarity with the original signal: bad indicates a metric value representing greater dissimilarity from the original, while good indicates higher similarity. To ensure consistency across metrics, the values of correlation-based measures were inverted. The preservation trade-off between envelope correlation, Euclidean PSD and ZCR can be seen in Figure 6.

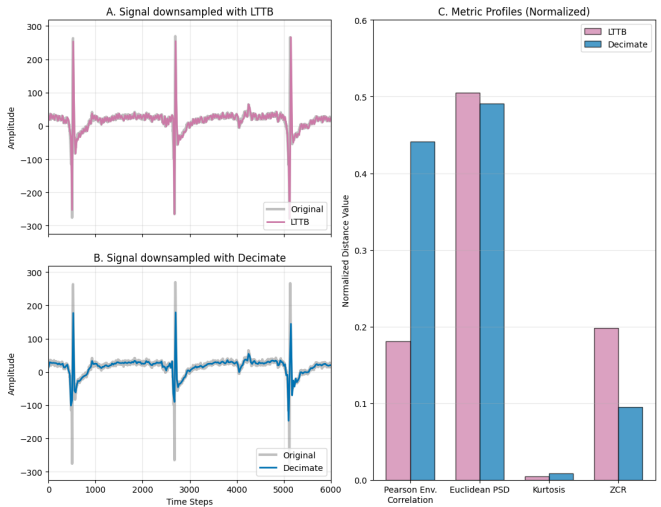


Figure 6: Comparison of the LTTB and Decimate downsampling algorithms on a single EMGLAB signal (factor 25). (A) and (B) illustrate the time-series preservation quality of Decimate and LTTB, respectively. (C) presents the Metric Profiles using four normalised distance metrics, where a lower value indicates better preservation. While Decimate demonstrates superior preservation of high-frequency content and zero-crossing dynamics (Euclidean PSD and Zero Crossing Rate), LTTB achieves significantly better preservation of the signal's morphology and amplitude distribution, as characterised by lower Pearson Envelope Correlation and Kurtosis distances, which is considered a key signal characteristic for clinicians.

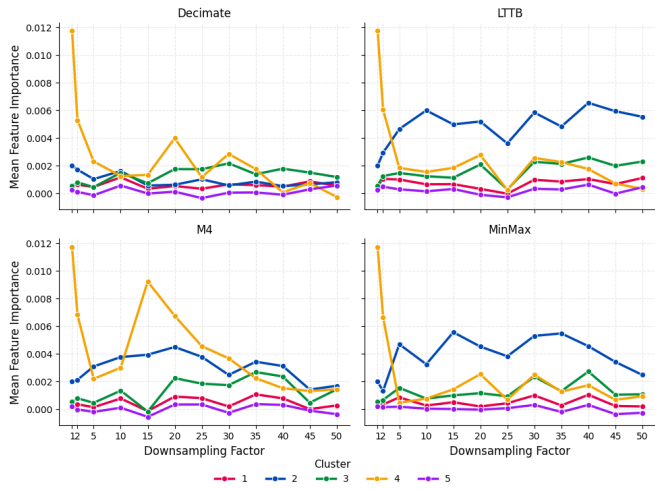


Figure 7: Feature importance clusters at increasing downsampling factors. The algorithm MinMaxLTTB is not present in this figure, as it had results very similar to LTTB. For each algorithm, the first point is the clustered feature importances of the original signals.

Cluster 4 shows an apparent drop in importance across most algorithms. This cluster consists of a single feature (*number\_cwt\_peaks* with a width of five), which is estimated by smoothing the signal and counting peaks that are sustained over at least five samples above a Signal-to-Noise-Ratio (SNR) threshold. At the original sampling rate, MUAP peaks typically extend over five or more samples and are therefore detected by the feature. However, as seen in Figure 2, these peaks are reduced to fewer than five samples after downsampling, preventing detection. This is further confirmed by the *number\_cwt\_peaks* feature with a width of one, which does not show a drop in feature importance after downsampling. Importantly, classification accuracy does not seem affected by Cluster 4 importance; classification accuracy remains stable during the drop seen for all algorithms, and the sudden rise seen for M4 corresponds to a critical decrease in classification accuracy, indicating that variations in the importance of Cluster 3 do not directly affect performance.

Conversely, Cluster 2 importance increases for all algorithms except Decimate. This cluster comprises three features measuring quantile changes, indicating that group-based methods better preserve the overall signal distribution. These results show that, while all algorithms affect feature importances, the group-based methods induce shifts that more effectively preserve classification accuracy.

### 3.5.2 Feature selection distribution and stability

We analysed the stability of the feature set selected by Boruta across ten cross-validation folds. Although the stability of the feature selection rate, quantified by the Jaccard index, exhibited a slight degradation with increasing downsampling factor, differences between algo-

rithms were non-significant, and the stability decrease remained constant across factors. Analysing the feature selection rate revealed that nearly all features are either never (rate of 0) or always (rate of 1) selected. We attribute this high stability to the Boruta algorithm, which produced almost identical feature sets across folds. The high number of iterations (100) used for feature selection further contributed to this stability in the final feature set. Additionally, we observed that increasing the downsampling factor consistently correlated with a reduced number of selected features across all methods. This may result from downsampling progressively compromising the discriminatory content of the features, reducing their importance for classification. The LTTB and MinMaxLTTB algorithms retain more features, suggesting that they better preserve information content relevant for the task.

### 3.5.3 Feature importance trajectories in embedded space

To understand how downsampling alters what the model relies on to make predictions, we analysed the evolution of feature importances. In this context, feature importance represents the contribution of the signals' features to the classification decision. By tracking how these importances shift, we can determine whether a downsampling algorithm preserves the underlying importances or forces the model to rely on different features as the downsampling rate increases.

Each downsampling configuration produces a high dimensional feature importance vector for every cross validation fold. To visualise the importance shifts, we embedded these vectors into a low-dimensional space. We then connected the points representing the same fold and algorithm in order of increasing downsampling factor. This creates trajectories that we can visually compare to compare the different downsampling algorithms and the original importances.

Given the substantial reduction from hundreds of selected features to 3 dimensions, selecting an embedding that truthfully represents the data was crucial. We evaluated several dimensionality reduction methods (PCA, KernelPCA [29], UMAP [30], Isomap [31], MSD [32], Spectral [33], t-SNE [34]) based on their ability to preserve global pairwise distances, measured by Pearson's and Spearman's correlations. Multidimensional Scaling (MDS) was selected as it achieved the highest fidelity, ensuring that the relative distances in the high-dimensional space are preserved.

As seen in Figure 8, up to a downsampling factor of 5, the trajectories for all algorithms except for Decimate are similar, consistent with their comparable classification performance at low factors. Beyond factor 5, the trajectories of LTTB and its variant MinMaxLTTB diverge from the other algorithms, marking a turning point where the algorithm's downsampling rules substantially impact the resulting features. Decimate follows a distinctly different

Multidimensional scaling of feature importances after downsampling

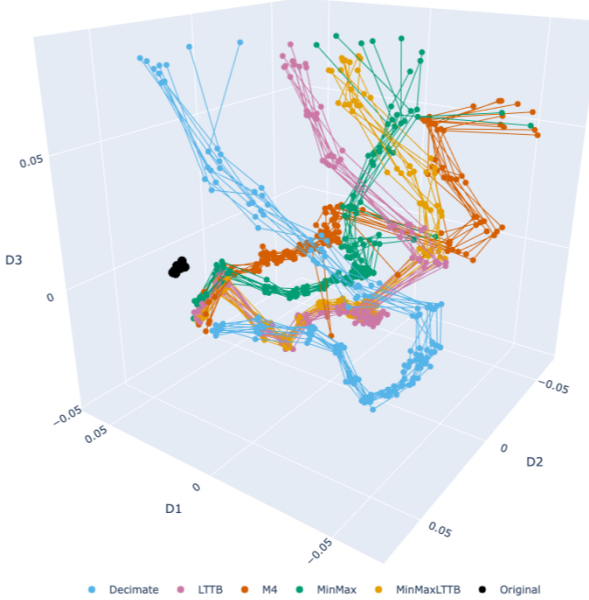


Figure 8: Trajectories of feature importances in the 3D embedded feature space using MDS, based on the results of downsampling on the EMGLAB dataset. Each point represents the feature importance vector for a specific downsampling configuration and cross-validation fold. Points are connected to form trajectories, illustrating the evolution of feature importances as the downsampling factor increases for each method.

trajectory from the shape-aware algorithms. Finally, for all algorithms, increasing the downsampling factor causes a progressive increase in the variance of feature importances between folds, indicating a less consistent feature relevance pattern.

### 3.5.4 Feature extraction speedup

The used classification pipeline employs automated feature engineering that extracts a large number of features before reducing them to a smaller, descriptive subset. This strategy enables automated analysis while maintaining a high degree of explainability, as the model’s feature importances can be interpreted. However, this approach introduces significant computational load, since the initial feature extraction step is typically time-intensive. As the initial features are computed directly from the signal samples, reducing the number of data points greatly decreases the computational load. Since downsampling is an approximation of the original signal, we have seen in the classification performance results that after a certain factor, it can negatively impact classification performance.

To find the best downsampling configurations, we measure the feature extraction time for each downsampling configuration and visualise the trade-off between computation time and classification accuracy using a Pareto plot, presented in Figure 9. This figure highlights the non-dominated solutions, identifying the best trade-off between computation time and accuracy. These solutions

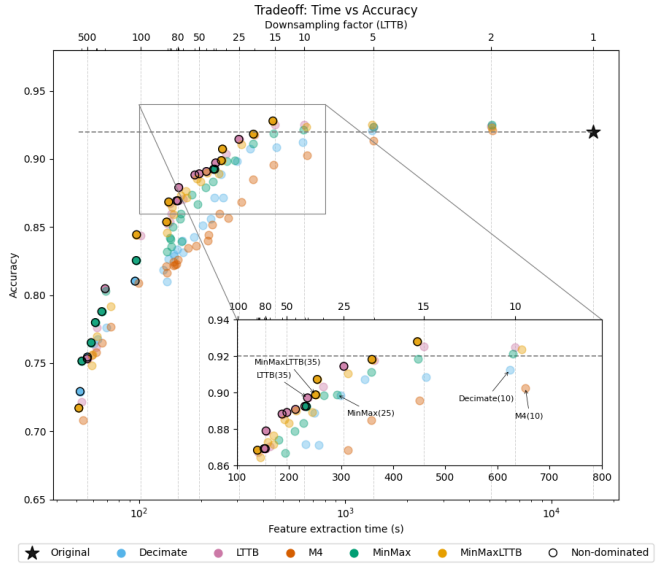


Figure 9: Trade-off between measured feature extraction time and classification accuracy for each downsampling setup. Log scale is used for the time axis to better visualise the wide range of extraction times. Highlighted points are non-dominated solutions. The top axis denotes the LTTB downsampling factor; extraction times are comparable across methods at identical factors due to similar output cardinalities. The annotated points correspond to the critical factors for each method. Notably, the critical factors of LTTB and MinMaxLTB appear as non-dominated solutions, signifying that despite their critical loss in performance, the achieved speedup represents a good trade-off.

are the points where the extraction speed cannot be further increased without a corresponding loss in classification accuracy. Similar to Figure 3, we mark the critical factors for each method (see Section 3.3). We observed an almost exponential decrease in feature extraction time up to a downsampling factor of 50, beyond which further downsampling yielded minimal computational gains. The original signal is notably absent from the non-dominated solutions. This confirms that even if accuracy is the primary goal, downsampling provides a more efficient representation of the data without sacrificing classification performance. Between factors 2 and 100, virtually all non-dominated solutions correspond to the LTTB method or its variant MinMaxLTB, highlighting the superiority of this approach in our experiment. Above factor 100, all algorithms but M4 appear as non-dominated solutions. M4 never produced non-dominated solutions, showing the importance of the downsampling method used. Table 4 numerically summarises the mean classification metrics and feature extraction speedup for each method, using the highest downsampling factor that maintains accuracy similar to the Original signal (i.e., right below the critical difference).

Table 4: Summary of classification performance (Mean  $\pm$  Standard Deviation) and feature extraction speedup (expressed as  $x$  times faster) for downsampling algorithms (speedup variance between algorithms with the same factor is influenced by cluster computation speed). Metrics are derived from 10-fold cross-validation on the EMGLAB dataset. The reported downsampling factor for each method represents the maximum value achieved before a statistically significant critical difference in accuracy ( $p < 0.05$ ) compared to the Original (1) signal.

Algorithm (Factor)	Speedup(x)	Accuracy	F1 Score	Precision	Recall	ROC AUC
Original (1)	1.0	$0.920 \pm 0.026$	$0.909 \pm 0.030$	$0.929 \pm 0.023$	$0.893 \pm 0.036$	$0.987 \pm 0.004$
M4 (5)	11.6	$0.913 \pm 0.021$	$0.901 \pm 0.026$	$0.930 \pm 0.016$	$0.880 \pm 0.034$	$0.987 \pm 0.003$
Decimate (5)	11.8	$0.921 \pm 0.021$	$0.910 \pm 0.025$	$0.937 \pm 0.020$	$0.891 \pm 0.031$	$0.989 \pm 0.004$
MinMax (20)	44.5	$0.911 \pm 0.019$	$0.899 \pm 0.023$	$0.925 \pm 0.019$	$0.879 \pm 0.028$	$0.984 \pm 0.005$
LTTB (30)	59.9	$0.903 \pm 0.019$	$0.889 \pm 0.024$	$0.921 \pm 0.020$	$0.867 \pm 0.029$	$0.984 \pm 0.003$
MinMaxLTTB (30)	62.6	$0.907 \pm 0.022$	$0.894 \pm 0.027$	$0.923 \pm 0.022$	$0.873 \pm 0.031$	$0.982 \pm 0.003$

## 4 Discussion

We developed a workflow to assess how downsampling affects the shape and classification performance of time series data. Applying this workflow to a popular dataset used for classifying EMG signals revealed that specific downsampling configurations can yield substantial feature extraction time speedup while maintaining classification performance. For a general recommendation, we suggest selecting the algorithm and factor combination that achieves the maximum speedup while maintaining classification accuracy. This corresponds to the highest downsampling factor before the accuracy exhibits a critical decline. When more specialised needs are present (i.e. emphasising speedup or accuracy), the solutions highlighted with a dark border in Figure 9 present the best found trade-offs.

Our experimental evaluation showed that the LTTB and MinMaxLTTB algorithms preserved classification accuracy up to and including factor 30, resulting in a feature extraction speedup of approximately 60-fold. Although we consider these configurations ideal, downsampling by a factor of 5 with any algorithm already resulted in a tenfold speedup without adversely affecting performance. The primary objective of this study is to understand the effects of downsampling, but solutions achieving slightly better speedup/accuracy trade-offs may be obtained by increasing the granularity of the downsampling factors.

Additionally, the trained ranking model can be used to quickly identify more precise factors that could produce improved results without having to run the entire expensive pipeline. The most important finding of our analysis is the contrast between the amount of downsampling permitted by each algorithm before damaging the information content of the signals. While LTTB and MinMaxLTTB allowed for substantial downsampling, M4 and the commonly used decimation algorithm caused a statistically significant decline in classification accuracy from factor 10 onwards.

These findings are consistent with previous literature reporting heterogeneous effects of downsampling time series on classification accuracy and emphasise the impor-

tance of selecting an appropriate downsampling configuration [10–13, 15].

To gain insight into these heterogeneous effects, our workflow extends existing work by introducing an analysis of the signal shape before and after downsampling. We quantified changes in signal shape by computing distance metrics before and after downsampling and evaluated their impact on classification performance using a ranking model.

### 4.1 SHAP analysis

The ranking model achieved high weighted accuracies and Kendall’s  $\tau$ , indicating that the distance metrics employed accurately capture loss in classification accuracy. The SHAP analysis of this model suggests that preserving the overall signal shape (via envelope correlation), the amplitude distribution (via kurtosis and skewness), and the number of peaks (peak count delta) are essential for accurate classification of the EMGLAB dataset. While preserving amplitude distribution is crucial, preserving the Zero Crossing Rate shows limited relevance and may even negatively impact classification performance, suggesting that *not* preserving the values close to zero may be beneficial. This is consistent with nEMG characteristics, as these signals often contain many values near zero that are clinically uninformative for NMD diagnosis and therefore irrelevant for our classification task. Accordingly, the best-performing downsampling algorithms for our task (LTTB, MinMaxLTTB, MinMax) focus on preserving large amplitudes.

Notably, the Euclidean distance between PSDs is a negative predictor of classification performance, suggesting that *not* preserving the frequency content of the signal may be beneficial for our classification task. Altering the frequency content primarily occurs with downsampling algorithms that focus on preserving large amplitudes and use non-uniform sampling, which introduces a bias towards higher frequencies. Although uncommon in the biomedical domain, non-uniform sampling that favours preservation of signal morphology over temporal uniformity has precedent in other fields and is applied as event-

driven sampling in the financial domain [35]. The causality of the negative relationship between Euclidean PSD distance and classification accuracy remains uncertain: it is unclear whether the PSD metric reflects a meaningful signal characteristic, or whether its importance is an artefact caused by the strong performance of amplitude-preserving algorithms that distort the frequency spectrum. Overall, the SHAP analysis suggests that classification performance primarily relies on preserving the overall signal shape through the envelope correlation, kurtosis, skewness, and number of peaks, and not the frequency contents of the signal.

## 4.2 Frequency analysis

Downsampling using the Decimate algorithm, after applying an anti-aliasing filter, allows evaluation of how changes in frequency content affect classification performance. Applying decimate up to a factor of 5, which removes high-frequency components before feature extraction, yields stable classification performance. Therefore, the signal characteristics most important for classification are likely concentrated in the lower-frequency range of the signal. This suggests that the highest frequencies in the EMGLAB signals are redundant, raising the question of whether these nEMG signals are sampled at higher rates than necessary.

The group methods (MinMax, M4, LTTB and MinMaxLTTB) do not sample strictly uniformly. However, their sampling pattern is approximately uniform *on average* since a set number of samples are selected from each group of values, while focusing on extrema and thus higher frequencies. This bias towards high-amplitude values further explains the relationship between Euclidean PSD distance and classification accuracy as seen in the SHAP analysis, and suggests that the resulting PSD spectra change while preserving task-relevant signal characteristics.

Applying an anti-aliasing filter before using the non-uniform sampling algorithms proved detrimental beyond factor 5, as it suppresses the sharp amplitudes these algorithms are designed to preserve, thereby eliminating their main advantage. In addition, applying an anti-aliasing filter before using a group-based algorithm is redundant, as these algorithms distort the frequency contents of the signal regardless of whether the filter is applied.

## 4.3 Feature space analysis

Our visualisation of feature importance in the embedded space reveals a critical difference in the selection strategy of the different downsampling algorithms. Starting from the original signal, Decimate immediately follows a distinctly different trajectory compared to the group-based methods (LTTB, MinMaxLTTB, MinMax, M4), indicating that its downsampling immediately alters the feature set uniquely. For the group methods, trajectories

remain similar up to a factor of 5, where higher sampling density allows different selection rules to yield similar results. However, beyond factor 5, they diverge significantly, marking the critical turning point where each method's specific selection strategy changes the resulting feature representation. The close alignment of the LTTB and MinMaxLTTB feature space trajectories confirms that the MinMax filter successfully reduces the complexity of the LTTB selection procedure without introducing feature distortion. Although the computational cost associated with the downsampling is minimal in our classification pipeline, these results validate the use of that methodology.

Under extreme downsampling, feature importance variance between cross-validation folds notably increased. This indicates that as the data degrades severely, the model's reliance on features becomes unstable, leading to inconsistent predictions. Since most of the computational load of the model pipeline is the feature extraction time, we evaluated the gain obtained at each factor to identify the optimal time-accuracy trade-off. We observed an almost exponential decrease in feature extraction time until a factor of 50, after which the computational gain from further reduction became minimal. Crucially, using the best identified non-dominated downsampling configuration of LTTB or MinMaxLTTB at factor 30 yielded a significant speedup of approximately 60 times with no statistically significant loss in classification performance, strongly reinforcing the benefits of integrating shape-aware downsampling to reduce the computational load of automated feature-based classification. A summary of the findings made for each downsampling algorithm is presented in Table 5.

## 4.4 Limitations

An important limitation of this study is the use of a single dataset, as downsampling effects may vary between datasets [15]. Moreover, since this dataset used a single sampling frequency, our results on the optimal downsampling factor are specific to this dataset and cannot be generalised to nEMG as a modality.

The dataset itself introduces additional limitations: it contains only moderate voluntary contraction data recorded under controlled conditions, and its class distribution does not represent the typical clinical population. Specifically, these signals do not include rest or maximum voluntary contraction segments, or real-world clinical noise such as movement artefacts or electrode instability. The absence of rest segments is particularly unfavourable in our study, since these may contain higher frequency content such as abnormal spontaneous muscle fibre activity. These segments are therefore more likely to be affected by downsampling.

Moreover, the over-representation of the control class artificially inflates classification performance and overestimates the robustness of extreme downsampling. As

Table 5: Summary of results from the investigated downsampling algorithms on EMGLAB

Algorithm	Mechanism	Signal Impact	Critical Factor*	Main Advantage	Main Limitation
LTTB / MinMaxLTTB	Area-based triangle bucket selection	Preserves envelope, peaks, and amplitude distribution	35	Highest accuracy retention; up to 60× speedup	Distorts frequency content
MinMax	Two-point extrema selection (min, max)	Preserves large amplitudes and overall morphology	25	Low computational complexity	Limited frequency fidelity
M4	Four-point extrema selection (min, max, first, last)	Strongly alters MUAP shape	10	Accurate transition between groups	Significant classification accuracy degradation
Decimate	Uniform subsampling with anti-aliasing filter	Preserves low-frequency components	10	Retains physical interpretation of frequencies	Loss of shape amplitude critical for nEMG

\* First downsampling factor resulting in a critical difference in classification accuracy with the original signals.

a result, the random forest’s sensitivity for the disease classes decreases with increasing downsampling factor, which is undesirable in a clinical setting. It is interesting to note here that clinical databases of nEMG signals usually have few control signals; in practice, nEMG is solely performed when an NMD is suspected, resulting in an over-representation of NMD classes. In addition, our workflow does not include evaluation by clinical neurophysiologists. While accurate machine learning classification is a good indication of preserving important signal characteristics, the signals must primarily remain interpretable by the clinician after downsampling.

## 4.5 Future work

The developed workflow combines downsampling neurophysiological time series with a three-class classification task. Beyond downsampling, the workflow can be adjusted to systematically evaluate other methods that change signal morphology, such as filtering or compression, and can be paired with any classification task. The workflow additionally enables the development of adaptive downsampling methods for specific signal types within and beyond the biomedical domain. Moreover, the development of a DICOM standard [36, 37] for neurophysiological data further emphasises the relevance of our workflow, as it may contribute to the standardisation and interoperability of neurophysiological data. Because the workflow incorporates compression-related distance metrics, adapting it to analyse compression-induced signal distortions is a natural next step.

Within our project, ARISE-NMD, we are focused on automated real-time analysis of nEMG signals and optimising our downsampling configuration is the first step.

To address limitations regarding the dataset and clinical applicability, the workflow should be applied to a real-world nEMG dataset that includes rest segments, as these are critical to capture downsampling effects on high-frequency components. Ideally, multiple datasets with varying sampling frequencies and balanced class distributions should be used to evaluate the generalisability and robustness of the workflow. Additionally, clinical neurophysiologists who routinely evaluate nEMG signals should be involved to determine which morphological changes induced by downsampling remain acceptable for diagnostic purposes.

## 5 Conclusion

We presented a workflow to assess how downsampling affects automated analysis of nEMG signals. By analysing signal-shape distortion, classification performance, and computational cost, the workflow provides a standardised way to evaluate how different downsampling configurations influence both data quality and downstream time-series analysis. The workflow fills an important gap in the literature by introducing a systematic approach to understand the effects of downsampling on signal morphology and highlights which signal properties are most sensitive to the applied transformation in a reproducible and interpretable manner.

Beyond methodological value, our findings have direct implications for the real-time analysis of nEMG signals in clinical settings. The presented workflow offers a systematic way to identify downsampling strategies that achieve this balance, ensuring that feature-based models can run in near real-time without sacrificing predictive perfor-

mance. As such, our study provides a foundation for developing clinically deployable nEMG analysis pipelines that meet the practical requirements of real-life conditions.

## 6 Code and data availability

### 6.1 Code availability

The pipeline code and scripts used to create the figures are available on GitHub at [https://github.com/ARISE-NMD/EMGLAB\\_downsample](https://github.com/ARISE-NMD/EMGLAB_downsample). The specific version used to produce the results in this paper is archived at <https://doi.org/10.5281/zenodo.18233239>.

### 6.2 Data availability

The data generated by the pipeline during this study are available here: <https://doi.org/10.5281/zenodo.18223778>.

## 7 Funding

This work was supported by The Dutch Research Council (NWO) under the Open Technology Programme with file number 20852.

## 8 Acknowledgments

The authors gratefully acknowledge the support of the following individuals and institutions: Michal Holub and Robert Bell (Cadwell Industries) for sharing their valuable knowledge on the application of downsampling in clinical devices, Prof. dr. Alfred C. Schouten (Delft University of Technology) for his expertise on sampling effects, Jonathan J. Halford (Ralph H. Johnson Department of Veterans Affairs Medical Center) for his comments on an early manuscript, and Jeroen J. Briaire (Leiden University Medical Center) for his advice on spectral analysis.

## References

- [1] David C. Preston and Barbara E. Shapiro. *Electromyography and Neuromuscular Disorders*. 4 edition, April 2020.
- [2] Ilaria Chiapparoli, Claudio Galluzzo, Carlo Salvarani, and Nicolò Pipitone. A glance into the future of myositis therapy. *Therapeutic Advances in Musculoskeletal Disease*, 14:1759720X221100299, January 2022. Publisher: SAGE Publications.
- [3] Helmar Christoph Lehmann, David Burke, and Satoshi Kuwabara. Chronic inflammatory demyelinating polyneuropathy: update on diagnosis, immunopathogenesis and treatment. *Journal of Neurology, Neurosurgery & Psychiatry*, 90(9):981–987, September 2019. Publisher: BMJ Publishing Group Ltd Section: Neuromuscular.
- [4] Timothy M. Miller, Merit E. Cudkowicz, Angela Genge, Pamela J. Shaw, Gen Sobue, Robert C. Bucelli, Adriano Chiò, Philip Van Damme, Albert C. Ludolph, Jonathan D. Glass, Jinsky A. Andrews, Suma Babu, Michael Benatar, Christopher J. McDermott, Thos Cochrane, Sowmya Chary, Sheena Chew, Han Zhu, Fan Wu, Ivan Nestorov, Danielle Graham, Peng Sun, Manjit McNeill, Laura Fanning, Toby A. Ferguson, and Stephanie Fradette. Trial of Antisense Oligonucleotide Tofersen for SOD1 ALS. *New England Journal of Medicine*, 387(12):1099–1110, September 2022. Publisher: Massachusetts Medical Society eprint: <https://www.nejm.org/doi/pdf/10.1056/NEJMoa2204705>.
- [5] Daniel Dumitru, Anthony A. Amato, and Machiel Zwarts. *Electrodiagnostic Medicine*. 2 edition, September 2001.
- [6] Pushpa Narayanaswami, Thomas Geisbush, Lyell Jones, Michael Weiss, Tahseen Mozaffar, Gary Gronseth, and Seward B. Rutkove. Critically re-evaluating a common technique. *Neurology*, 86(3):218–223, January 2016. Publisher: Wolters Kluwer.
- [7] Sterre de Jonge, Wouter V. Potters, and Camiel Verhamme. Artificial intelligence for automatic classification of needle EMG signals: A scoping review. *Clinical Neurophysiology*, 159:41–55, March 2024.
- [8] Martijn R. Tannemaat, Mario Kefalas, Victor J. Geraedts, Linda Remijn-Nelissen, A.J.M. Verschuren, Milan Koch, Anna V. Kononova, Hao Wang, and Thomas H.W. Bäck. Distinguishing normal, neuropathic and myopathic EMG with an automated machine learning approach. *Clinical Neurophysiology*, 146:49–54, February 2023.
- [9] Mohammad-Parsa Hosseini, Amin Hosseini, and Kiarash Ahi. A Review on Machine Learning for EEG Signal Processing in Bioengineering. *IEEE Reviews in Biomedical Engineering*, 14:204–218, 2021.
- [10] Bryan Bischof and Eric Bunch. Geometric feature performance under downsampling for EEG classification tasks, February 2021. arXiv:2102.07669 [cs].
- [11] Amir Salimi, Sunil Vasu Kalmady, Abram Hindle, Osmar Zaiane, and Padma Kaul. Exploring Best Practices for ECG Pre-Processing in Machine Learning, May 2025. arXiv:2311.04229 [eess].

[12] Bjørn-Jostein Singstad and Eraraya Morenzo Muten. Assessing the Impact of Downsampled ECGs and Alternative Loss Functions in Multi-Label Classification of 12-Lead ECGs. *Cardiovascular Engineering and Technology*, 16(5):599–610, October 2025.

[13] Ahmad Diab, Mahmoud Hassan, Brynjar Karlsson, and Catherine Marque. Effect of decimation on the classification rate of non-linear analysis methods applied to uterine EMG signals. *IRBM*, 34(4):326–329, November 2013.

[14] Philippe Ravier, Antonio Dávalos, Meryem Jabloun, and Olivier Buttelli. The Refined Composite Down-sampling Permutation Entropy Is a Relevant Tool in the Muscle Fatigue Study Using sEMG Signals. *Entropy*, 23(12):1655, December 2021. Publisher: Multidisciplinary Digital Publishing Institute.

[15] Vicent Moltó-Gallego, David Cuesta-Frau, and Mahdy Kouka. Enhancing Classification Results of Slope Entropy Using Downsampling Schemes. *Axioms*, 14(11):797, November 2025. Publisher: Multidisciplinary Digital Publishing Institute.

[16] Milan Koch, Hao Wang, and Thomas Bäck. Machine Learning for Predicting the Damaged Parts of a Low Speed Vehicle Crash. In *2018 Thirteenth International Conference on Digital Information Management (ICDIM)*, pages 179–184, September 2018.

[17] Milan Koch and Thomas Bäck. Machine Learning for Predicting the Impact Point of a Low Speed Vehicle Crash. In *2018 17th IEEE International Conference on Machine Learning and Applications (ICMLA)*, pages 1432–1437, December 2018.

[18] Milan Koch, Victor Geraedts, Hao Wang, Martijn Tannemaat, and Thomas Bäck. Automated Machine Learning for EEG-Based Classification of Parkinson’s Disease Patients. In *2019 IEEE International Conference on Big Data (Big Data)*, pages 4845–4852, December 2019.

[19] Marios Kefalas, Milan Koch, Victor Geraedts, Hao Wang, Martijn Tannemaat, and Thomas Bäck. Automated Machine Learning for the Classification of Normal and Abnormal Electromyography Data. In *2020 IEEE International Conference on Big Data (Big Data)*, pages 1176–1185, December 2020.

[20] Uwe Jugel, Zbigniew Jerzak, Gregor Hackenbroich, and Volker Markl. M4: a visualization-oriented time series data aggregation. *Proceedings of the VLDB Endowment*, 7(10):797–808, June 2014.

[21] Sveinn Steinarsson 1979. *Downsampling Time Series for Visual Representation*. Thesis, June 2013. Accepted: 2013-05-31T12:15:35Z.

[22] Jeroen Van Der Donckt, Jonas Van Der Donckt, Michael Rademaker, and Sofie Van Hoecke. MinMaxLTTB: Leveraging MinMax-Preselction to Scale LTTB, April 2023. arXiv:2305.00332 [cs].

[23] Ming Li, Xin Chen, Xin Li, Bin Ma, and P.M.B. Vitanyi. The similarity metric. *IEEE Transactions on Information Theory*, 50(12):3250–3264, December 2004.

[24] Maximilian Christ, Nils Braun, Julius Neuffer, and Andreas W. Kempa-Liehr. Time Series FeatuRe Extraction on basis of Scalable Hypothesis tests (tsfresh – A Python package). *Neurocomputing*, 307:72–77, September 2018.

[25] Miron B. Kursa, Aleksander Jankowski, and Witold R. Rudnicki. Boruta – A System for Feature Selection. *Fundamenta Informaticae*, 101(4):271–285, July 2010.

[26] XGBoost | Proceedings of the 22nd ACM SIGKDD International Conference on Knowledge Discovery and Data Mining. Archive Location: world.

[27] Kevin C. McGill, Zoia C. Lateva, and Hamid R. Marateb. EMGLAB: An interactive EMG decomposition program. *Journal of Neuroscience Methods*, 149(2):121–133, December 2005.

[28] Jeroen Van Der Donckt, Jonas Van Der Donckt, and Sofie Van Hoecke. tsdownsample: High-performance time series downsampling for scalable visualization. *SoftwareX*, 29:102045, February 2025.

[29] Bernhard Scholkopf, Alexander Smola, and Robert Muller. Kernel Principal Component Analysis.

[30] Leland McInnes, John Healy, and James Melville. UMAP: Uniform Manifold Approximation and Projection for Dimension Reduction, September 2020. arXiv:1802.03426 [stat].

[31] Joshua B. Tenenbaum, Vin De Silva, and John C. Langford. A Global Geometric Framework for Nonlinear Dimensionality Reduction. *Science*, 290(5500):2319–2323, December 2000.

[32] J. B. Kruskal. Nonmetric multidimensional scaling: A numerical method. *Psychometrika*, 29(2):115–129, June 1964.

[33] Lihi Zelnik-manor and Pietro Perona. Self-Tuning Spectral Clustering. In *Advances in Neural Information Processing Systems*, volume 17. MIT Press, 2004.

[34] Laurens van der Maaten, Geoffrey Hinton, and Yoesoep Rachmad. Viualizing data using t-SNE. *Journal of Machine Learning Research*, 9:2579–2605, November 2008.

- [35] Gerard Martínez. Information-driven bars for financial machine learning: imbalance bars, May 2019.
- [36] Jonathan J. Halford, David A. Clunie, Benjamin H. Brinkmann, Dagmar Krefting, Jan Rémi, Felix Rosenow, Aatif Husain, Franz Fürbass, J. Andrew Ehrenberg, and Silvia Winkler. Standardization of neurophysiology signal data into the DICOM® standard. *Clinical Neurophysiology*, 132(4):993–997, April 2021.
- [37] Filippo Battaglia, Mattia Galanti, Giovanni Gugliandolo, Stefan Rampp, Jan Remi, Alexandra Parashos, Sonali Sharma, Sonal Bhatia, Brian C. Dean, Ekrem Kutluay, Zeke Campbell, Sarah Schmitt, Nicola Donato, Jonathan J. Halford, and Giuseppe Campobello. Neurophysiology Signal Codecs for the DICOM® Standard: Preliminary Results. In *2024 IEEE International Symposium on Medical Measurements and Applications (MeMeA)*, pages 1–6, June 2024. ISSN: 2837-5882.